Investigating lymphangiogenesis in vitro and in vivo using engineered human lymphatic vessel networks

Shira Landau[a], Abigail Newman[a], Shlomit Edri[a], Inbal Michael[a], Shahar Ben-Shaul[a], Yulia Shandalov[a], Tom Ben-Arye[a,b], Pritinder Kaur[c], Ming H. Zheng[d], and Shulamit Levenberg[a,1]

[a]Department of Biomedical Engineering, Technion – Israel Institute of Technology, Haifa 32000, Israel; [b]Russell Berrie Nanotechnology Institute, Technion – Israel Institute of Technology, Haifa 32000, Israel; [c]School of Biomedical Sciences, Curtin University, Perth 6845, WA, Australia; and [d]Brain and Bone Research, Perron Institute for Neurological and Translational Science, Perth 6009, WA, Australia

Edited by Robert Langer, Massachusetts Institute of Technology, Cambridge, MA, and approved June 28, 2021 (received for review January 30, 2021)

The lymphatic system is involved in various biological processes, including fluid transport from the interstitium into the venous circulation, lipid absorption, and immune cell trafficking. Despite its critical role in homeostasis, lymphangiogenesis (lymphatic vessel formation) is less widely studied than its counterpart, angiogenesis (blood vessel formation). Although the incorporation of lymphatic vasculature in engineered tissues or organoids would enable more precise mimicry of native tissue, few studies have focused on creating engineered tissues containing lymphatic vessels. Here, we populated thick collagen sheets with human lymphatic endothelial cells, combined with supporting cells and blood endothelial cells, and examined lymphangiogenesis within the resulting constructs. Our model required just a few days to develop a functional lymphatic vessel network, in contrast to other reported models requiring several weeks. Coculture of lymphatic endothelial cells with the appropriate supporting cells and intact PDGFR-β signaling proved essential for the lymphangiogenesis process. Additionally, subjecting the constructs to cyclic stretch enabled the creation of complex muscle tissue aligned with the lymphatic and blood vessel networks, more precisely biomimicking native tissue. Interestingly, the response of developing lymphatic vessels to tensile forces was different from that of blood vessels; while blood vessels oriented perpendicularly to the stretch direction, lymphatic vessels mostly oriented in parallel to the stretch direction. Implantation of the engineered lymphatic constructs into a mouse abdominal wall muscle resulted in anastomosis between host and implant lymphatic vasculatures, demonstrating the engineered construct's potential functionality in vivo. Overall, this model provides a potential platform for investigating lymphangiogenesis and lymphatic disease mechanisms.

lymphangiogenesis | lymphatic endothelial cells | vascularization | engineered tissue

The lymphatic and blood vascular systems are two distinct vessel network systems that work in synchrony to maintain tissue homeostasis. Blood vessels transport oxygen and nutrients around the body, while lymphatic vessels collect leaked fluid and macromolecules from the interstitial space and return them to the blood circulation, maintaining interstitial fluid homeostasis (1). Furthermore, the lymphatic system plays a central role in immune responses, inflammation regulation, and lipid absorption (2). While many in vitro models have been created to study angiogenesis, fewer attempts have been made to engineer an in vitro platform to study lymphangiogenesis. Such engineered models are critical for both fundamental research and the development of clinically implantable tissue to treat various diseases involving the lymphatic system. One such disease is lymphedema, a chronic condition that affects 200 million people worldwide (3). Lymphedema is characterized by tissue swelling resulting from a compromised lymphatic system. The condition is mainly caused by complications during cancer treatment but may also develop due to genetic disorders. The condition is progressive and incurable, with a high risk of infection. Implantation of engineered lymphatic tissue can serve as a treatment for such disease (4).

Lymph flow is primarily driven by pressures generated by lymphatic contractions of the smooth muscle cells surrounding the vessels (5). Impaired contractility thus reduces lymph flow and may cause lymphedema. Previous computational studies have investigated the correlation between lymphatic vessel contractility and mechanical stimulation, such as mechanical loading, pressure gradients, and shear stress amplitudes (6, 7). Furthermore, studies have investigated lymphatic vessel capacity to distend under mechanical loading conditions. In addition, the microenvironment composition has been shown to play an important role in enabling lymphatic vessel functionality (4).

Thus far, several groups have been able to engineer lymphatic tissues. Marino et al. created dermo-epidermal skin grafts with lymphatic and blood vessels embedded in a fibrin-collagen gel (8). Others created a lymphatic vessel network within multilayered fibroblast sheets (9, 10). Another study demonstrated that different hydrogel compositions are required for the optimal growth and development of blood and lymphatic endothelial cells (BECs and LECs, respectively) (11). However, no studies have investigated the influence of the supporting cells, the secreted extracellular matrix (ECM), and the mechanical environment on the forming lymphatic vessels. Since lymphatic pathologies are known to correlate with mechanically impaired lymphatic vessels (4), it is important to create lymphatic models with a biomimetic microenvironment.

Significance

Lymphatic vessel networks are important for various biological processes; thus, incorporating them into engineered constructs can have both research and clinical implications. Engineered lymphatic vessels can improve biomimicry and functionality of in vitro tissue assays and serve as a treatment for various diseases associated with impaired lymphatic function. In this work, we created functional engineered lymphatic vessels that anastomosed to the host lymphatic system postimplantation. We investigated the effect of supporting cells, cell-secreted extracellular matrix, and mechanical forces on lymphatic vessel formation within engineered constructs. Interestingly, lymphatic vasculature responded differently to cyclic stretch compared to blood vasculature. This phenomenon opens up an avenue for investigating the variability of cellular responses to mechanical stimulation.

Author contributions: S. Landau, A.N., I.M., S.B.-S., Y.S., T.B.-A., and S. Levenberg designed research; S. Landau, A.N., I.M., S.B.-S., Y.S., and T.B.-A. performed research; P.K., M.H.Z., and S. Levenberg contributed new reagents/analytic tools; S. Landau, A.N., S.E., and S. Levenberg analyzed data; and S. Landau, A.N., and S. Levenberg wrote the paper.

Competing interest statement: M.H.Z. is the consultant chief scientific officer of Orthocell.

This article is a PNAS Direct Submission.

[1]To whom correspondence may be addressed. Email: shulamit@bm.technion.ac.il.

This article contains supporting information online at https://www.pnas.org/lookup/suppl/doi:10.1073/pnas.2101931118/-/DCSupplemental.

Published July 29, 2021.

In this study, lymphatic vessel networks were engineered to investigate fundamental questions concerning lymphangiogenesis, including the influence of different supporting cells on the formation of lymphatic vessels and the role of PDGFR-β, an important receptor associated with support cells recruitment, in vessel formation. In addition, a complex tissue designed to better mimic native tissue was generated and lymphatic and blood vessel development along with muscle formation were monitored. In addition, the impact of the application of cyclic stretch on the organization and alignment of lymphatic-blood-vessel-muscle tissue was assessed. Finally, the penetration and anastomosis of the engineered lymphatic vessels were monitored following their implantation into mice.

Results

Dental Pulp Stem Cells Are Superior to Other Supporting Cells in Inducing Lymphatic Vessel Formation. LECs were seeded with supporting cells on CelGro collagen scaffolds. Unlike gels that tend to shrink and rupture (12), these scaffolds are mechanically stable, enabling easy implantation and preventing vessel deformation. As previously reported (9–11), supporting cells are required to engineer lymphatic vessels, as confirmed here in constructs lacking supporting cells in the culture, which showed no vessel formation and LECs remained as single cells (*SI Appendix*, Fig. S2). As most prior reports of engineered lymphatic vessels used fibroblasts as supporting cells (9–11), we initially cultured fibroblasts with the fluorescently labeled LECs within the CelGro sheet. At 2 d postseeding, confocal imaging showed vessel development. However, 3 d later, vessels had degraded and disappeared (Fig. 1 *A* and *B*). Use of pericytes as supporting cells enabled the formation of an LEC vessel network (*SI Appendix*, Fig. S3).

We previously reported (13) that dental pulp stem cells (DPSCs) contribute to blood vessel formation; therefore, they were examined here for their potential to support lymphatic vessel formation. LECs cocultured with DPSCs developed more elongated and stable vessels than those cocultured with fibroblasts or pericytes (Fig. 1 *A* and *B*). Additionally, in constructs containing fibroblast, a layer composed of single cells appeared on the construct surface, indicating that the cells failed to form vessels in this region. Vessels were present mainly in the inner scaffold region, whereas in the DPSC-containing constructs, no such cell layer appeared, and all LECs were assembled into vessels (Fig. 1*C*), demonstrating that DPSCs have a significant advantage over fibroblasts in supporting lymphatic vessel formation.

To further understand the reason for these differences, we stained the fibroblast and DPSC constructs for the ECM markers collagen-I and collagen-IV, to determine if ECM secretion by the supporting cells underlies these differences. Confocal imaging revealed expression differences between the constructs in the surface and inner regions (Fig. 1*D*). Constructs bearing fibroblasts showed dense coverage of both collagen-I and collagen-IV on their surface, while in DPSC constructs, this layer had more dispersed collagen coverage. In the inner region, constructs with fibroblast showed dense collagen-I expression, which filled the entire construct, and collagen-IV was located mainly around the vessel, whereas in the DPSC constructs, both collagens were localized near the forming vessels. Quantification of DAPI revealed higher DPSC concentrations in the surface area (*SI Appendix*, Fig. S4). The dense collagen layers within the fibroblast constructs contained gaps within the different layers, indicating excessive stress within these layers that could be the reason for LEC failure to form stable vessels within these constructs.

To further characterize the differences between the two supporting cell types, α-smooth muscle actin (α-SMA), an indicator of supporting cells differentiation and recruitment toward the forming vessels, was stained. α-SMA expression was found to be higher in constructs bearing DPSCs as opposed to those carrying fibroblasts. Moreover, while in fibroblast constructs, α-SMA fibers were sparse and located between the single-cell LECs, α-SMA morphology in the DPSC constructs was elongated but did not wrap the forming lymphatic vessels (Fig. 1*D*).

A cytokine array analysis of the cell medium collected on days 4 and 7 postseeding (Fig. 1*E*) identified higher VEGF-A secretion in constructs with DPSCs as compared to those with fibroblasts. In addition, constructs with DPSCs displayed an elevated leptin expression on day 4. Ang-2 and HGF secretion levels were not different between the two constructs on day 4 but were elevated in the fibroblast constructs on day 7. Inhibition of VEGFR using SU5416 caused LECs to remain as single cells that barely formed any vessels. Application of α-angiogenin antibody resulted in less vessel formation when compared to the control, and α-HGFR antibody resulted in shorter vessel elements that were less connected to each other, as indicated by a higher number of vessels' endpoints compared to the control (*SI Appendix*, Fig. S5).

To better understand the role of DPSCs in supporting lymphatic vessel formation, we performed an RNA-Sequencing (RNA-seq) experiment where RNA was extracted from constructs seeded with LECs with and without DPSCs. Analysis of genes that were significantly different (adjusted P value > 0.05) and with fold change above 5 showed that the three samples of the two groups clustered together (Fig. 2*A* and *SI Appendix*, Fig. S6). Analysis of enriched pathways of the up-regulated genes of the coculture group revealed that the most enriched pathways were associated with ECM and integrins. Whereas enriched pathways of the down-regulated genes were associated with abnormal lymphatic vessels and endothelial cell morphology (Fig. 2*B*). We then examined the enrichment pathways of the top 40 genes with the highest fold change; pathways were associated with VEGFR3 signaling, integrins, and PDGFR signaling (Fig. 2*C*).

The Role of PDGFR-β in Lymphatic and Blood Vessel Formation. To further assess the role of supporting cells in the formation of lymphatic vessels, PDGFR-β, a key receptor that recruits the supporting cells to the forming vessels, and whose ligand, PDGF-BB, is known as a lymphangiogenesis stimulator (14), was knocked down in DPSCs using electroporation-mediated CRISPR editing. Western blot analysis demonstrated an ∼50% decrease in protein expression following knockdown (KD) (*SI Appendix*, Fig. S1 *B* and *C*). As expected, in the wild-type control DPSC-LEC constructs, vessels began to form on day 1 and were fully developed on day 7. In constructs bearing PDGFR-β-KD DPSCs, LECs failed to form a stable vessel network; on day 1 the cells remained as single cells with a few clusters, and on day 7, the cells formed short and irregular vessels with few branching points (Fig. 3 *A*–*D*). As in the construct bearing a fibroblast-LEC coculture (Fig. 1*C*), the PDGFR-β-KD DPSC-LEC constructs had a single-cell monolayer on the scaffold surface, while vessels appeared only in the inner part (Fig. 3*C*).

Collagen-I and IV deposition was dispersed in the KD group. In contrast, in the control group, the collagens colocalized with the forming vessels, suggesting that the lack of PDGFR-β hinders basement membrane formation. Additionally, in the PDGFR-β-KD DPSCs, α-SMA showed aberrant morphology (Fig. 3*D*). A cytokine array showed elevated secretion of VEGF, angiogenin, and HGF in the control group on day 7 postseeding, when compared to the PDGFR-β-KD DPSC culture.

Lymphatic Vessel Characteristics and Functionality. The forming vessel network of LECs and DPSCs coculture within the CelGro scaffold displayed lymphatic characteristics with thick vessels, blind-end sacs, and lumens (Fig. 4 *A*–*D*). LECs were positively stained for the lymphatic marker LYVE-1 (Fig. 4*E*).

To assess the capacity of the engineered lymphatic vessels to collect fluid from the interstitium, Evans blue dye was injected into the construct. Confocal imaging captured 10 min after incubation showed the dye to be localized within the engineered lymphatic vessels (Fig. 4*F*), demonstrating their ability to collect fluid from the surroundings.

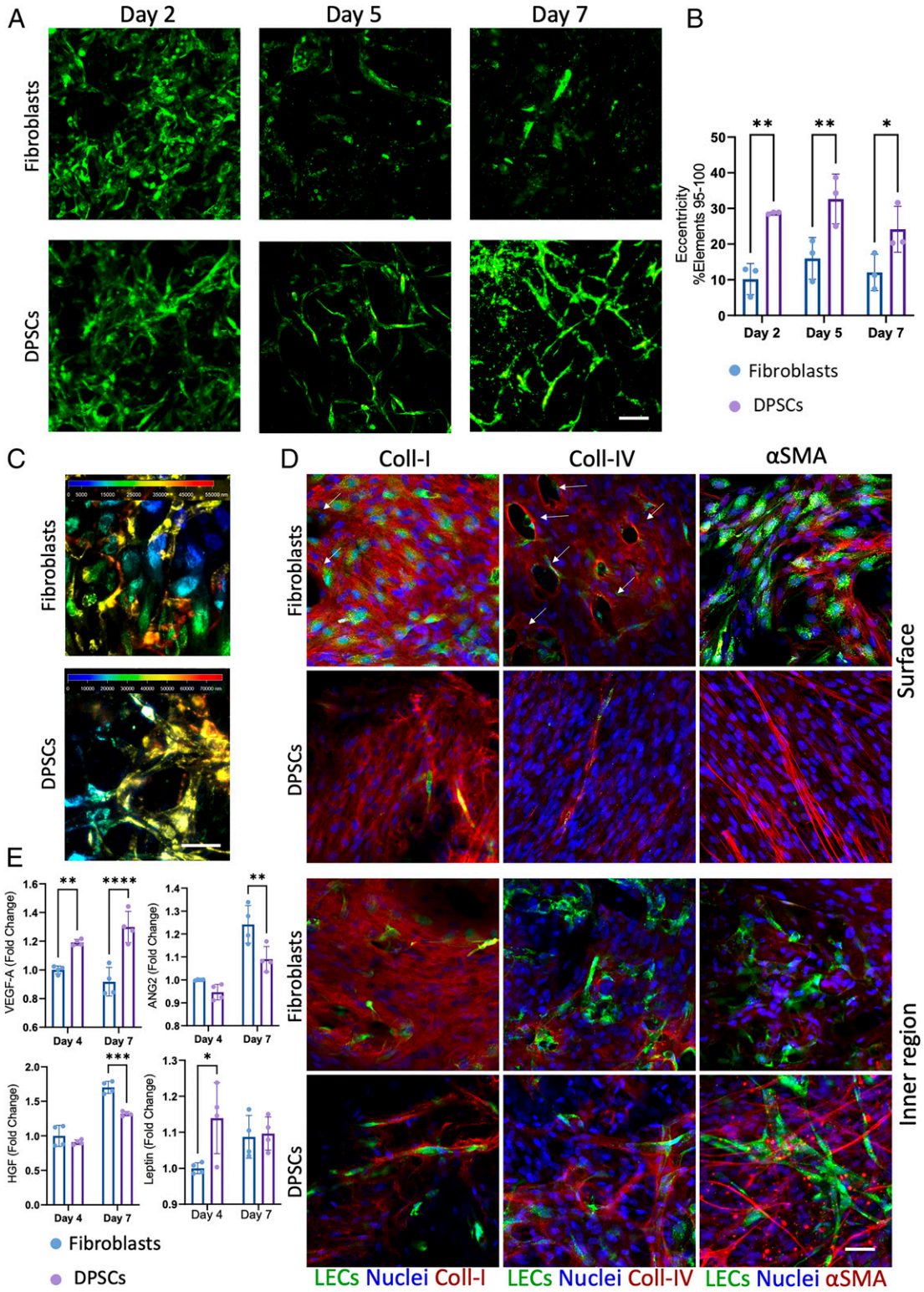

Fig. 1. Supporting cells affect lymphatic vessel formation. (*A*) LECs (green) were cocultured with fibroblasts (*Upper*) or DPSCs (*Lower*). Images were taken at 2, 5, and 7 d postseeding. (Scale bar, 50 μm.) (*B*) Eccentricity analysis demonstrating lymphatic vessel quality. (*C*) Depth color-coded projection of a confocal image of the lymphatic vessel; cool/warm colors indicate near/far from the surface, respectively. (Scale bar, 50 μm.) (*D*) Confocal images of fibroblast- and DPSC-bearing constructs grown for 7 d and immunofluorescently stained for α-SMA and collagen-I and -IV. The *Upper* and *Lower* show representative images of the surface and inner regions, respectively. (Scale bar, 50 μm.) (*E*) Cytokine secretion profiles of the two construct types, as measured in medium collected on days 4 and 7 postseeding. The presented data are normalized to the profile of the fibroblast-bearing constructs on day 4. Error bars show the SEM (SEM). $^{*}P < 0.05$, $^{**}P < 0.01$, $^{***}P < 0.001$.

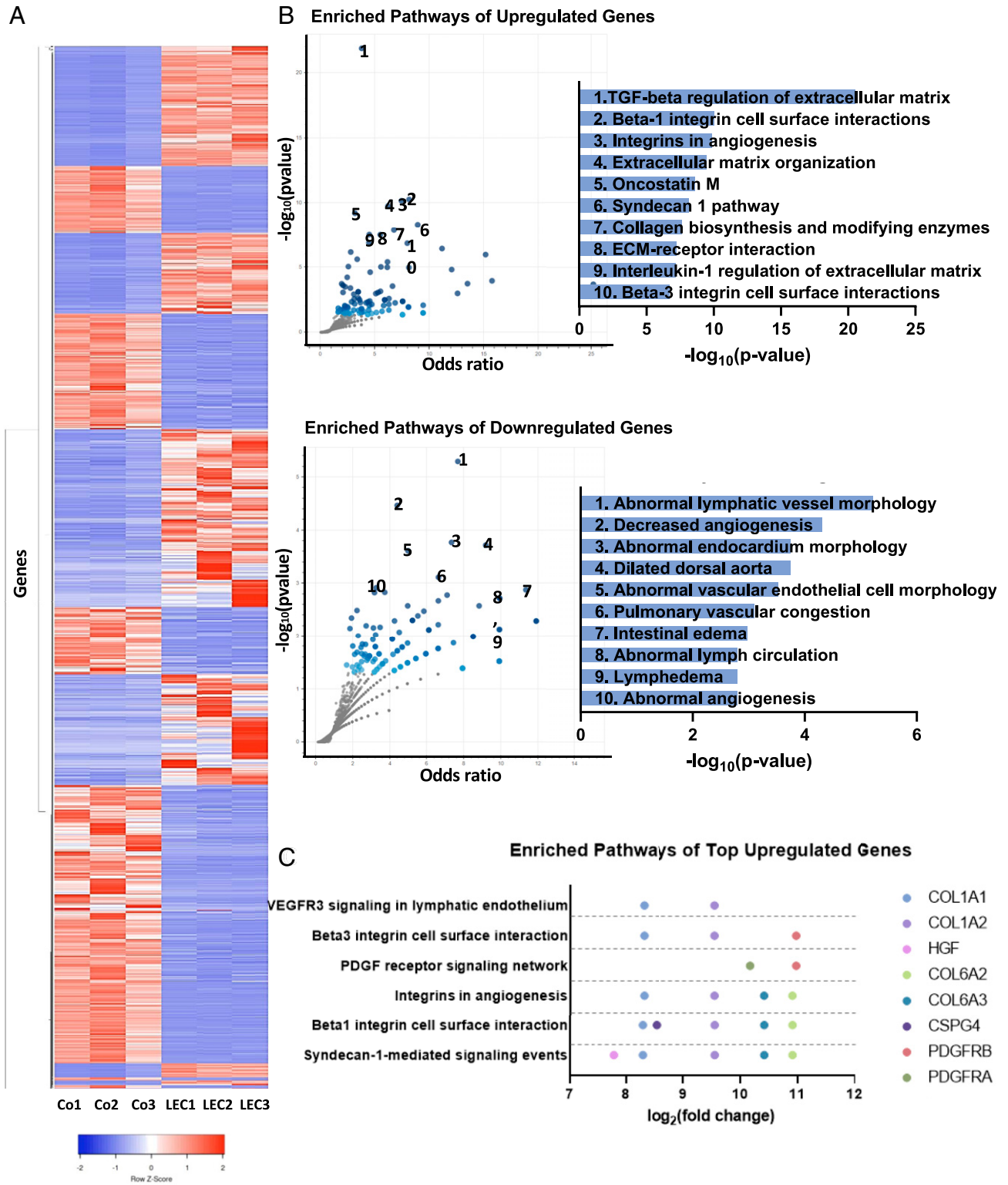

Fig. 2. Increased ECM expression by supporting cells enhances the forming of lymphatic vasculature. (*A*) Heatmap of genes of LEC constructs with DPSCs (Co) and without DPSCs (LEC) with expression fold change from the coculture group >5 and <−5. (*B*) The most enriched pathways of the genes are presented in *A*, where the *Upper* shows the up-regulated genes (in the coculture group, fold change >5) and the *Lower* shows the down-regulated genes (in the coculture group, fold change <−5). (*C*) *y*-axis shows enriched pathways of the 40 up-regulated genes with the highest fold change, and the *x*-axis shows the $\log_2$ (fold change) of the genes involved in the pathways.

Constructing a Complex Tissue: Incorporating BECs with LECs. To advance the current engineered tissue and create a more complex tissue, more precisely mimicking native tissue, BECs were added to the culture. This cell combination formed separate lymphatic and blood vessel networks (Fig. 5 *A*, *i*, *B*, and *C*, *i*); however, a few connecting points between the two networks were detected. The

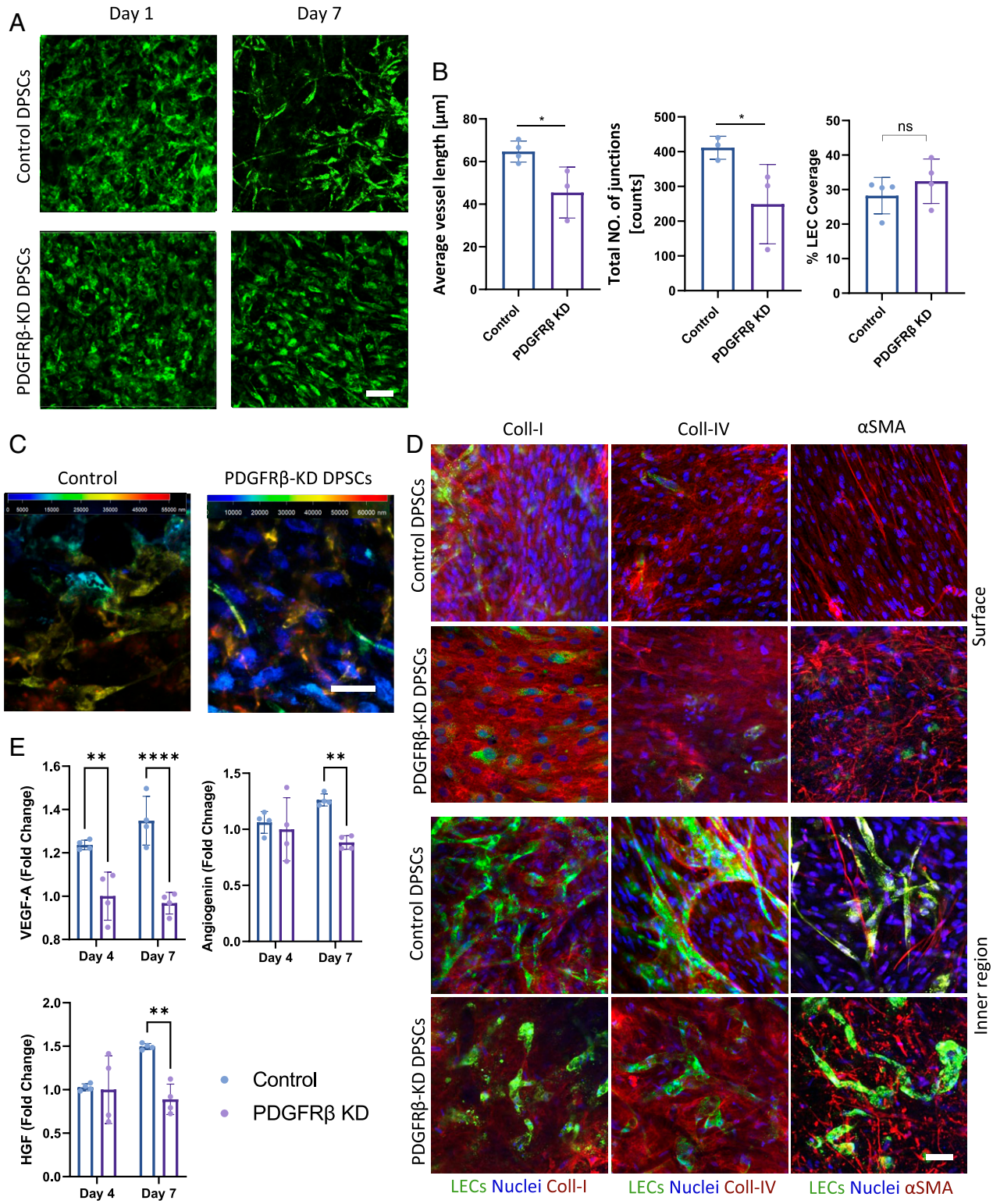

Fig. 3. PDGFR-β KD in DPSCs affects lymphatic vessel formation. (*A*) LECs (green) cocultured with wild-type (WT; upper panel) or PDGFR-β-KD (*Lower*) DPSCs. Images were taken on days 1 and 7 postseeding. (Scale bar, 100 μm.) (*B*) Vessel analysis by the AngioTool software demonstrating lymphatic vessel quality (analysis was performed on day 7 of culture). (*C*) Depth color-coded projection of a confocal image of the lymphatic vessels cultured for 7 d with WT DPSCs or PDGFR-β-KD DPSCs; cool/warm colors indicate near/far from the surface, respectively. (Scale bar, 50 μm.) (*D*) Confocal images of WT DPSC and PDGFR-β-KD DPSC constructs were grown for 7 d and immunofluorescently stained for α-SMA and collagen-I and -IV. The *Upper* and *Lower* show representative images of the surface and inner regions, respectively. (Scale bar, 50 μm.) (*E*) Cytokine secretion profiles of the two construct types in medium collected on days 4 and 7 postseeding. Error bars show SEM. $*P < 0.05$, $**P < 0.01$, $***P < 0.001$. ns, not significant.

vessels started to form on day 1 and were fully developed by day 7. In contrast, in PDGFR-β-KD DPSC-BEC-LEC constructs, both types of ECs failed to form a vessel network; on day 1, the cells remained as single cells and on day 7, the cells formed clusters with a few networks (Fig. 5*C*). Immunofluorescence staining of collagen-I and -IV was detected around both lymphatic and blood vessels in DPSC-BEC-LEC constructs; laminin and α-SMA staining was mainly detected within cells enveloping the blood vessels but not around lymphatic vessels (Fig. 5*B*). Finally, to fabricate complex muscle tissue containing lymphatic and blood vessels, LECs, BECs, DPSCs, and myoblasts were cultured on a single construct. Desmin staining of these constructs revealed myotube formation as well as lymphatic and blood vessel networks (Fig. 5*D*).

Lymphatic Vessel Alignment under Cyclic Stretch Differs from the Alignment of Blood Vessels, Muscle Cells, and Supporting Cells Due to Spatial Location Differences. Understanding mechanotransduction in lymphangiogenesis can contribute to the understanding of diseases in which lymphatic vessels are exposed to abnormal mechanical stress. We have previously shown that BECs form blood vessels that align under cyclic stretching (15–17). This alignment was mediated by the supporting cells in the culture, and both supporting cells and blood vessel networks aligned perpendicularly to the stretching direction.

We, therefore, aimed to examine LECs under cyclic stretching. When LECs were cocultured with DPSCs and cyclically stretched (Fig. 6*A*), the LECs located on the construct surface remained as single cells with a slight alignment perpendicular to the stretching direction. Deeper layers in the scaffold showed two-vessel network populations, one aligned perpendicularly and the other parallel to the stretching direction, with the dominance of the parallel-aligned population.

Upon addition of BECs to LEC-DPSC cocultures (Fig. 6*B*), BECs behaved as expected, forming vessels that aligned perpendicularly to the stretching direction. In contrast, the LECs did not form vessels and remained as single elongated cells in the surface regions, whereas deeper in the scaffold, they formed vessels that were mostly aligned in parallel to the stretching direction, with very few aligned perpendicularly.

To further mimic a native tissue that naturally experiences stretch in the body, we cultured the LECs and BECs with DPSCs and myoblasts. Interestingly, myoblast alignment was similar to that of BECs and DPSCs; they aligned perpendicular to the stretching direction (Fig. 6*C*).

To better understand the biological processes behind the morphological differences in cell responses to stretch, the proteomes of cocultures of LECs with DPSCs and BECS with DPSCs under cyclic stretch were analyzed by mass spectrometry (*SI Appendix*,

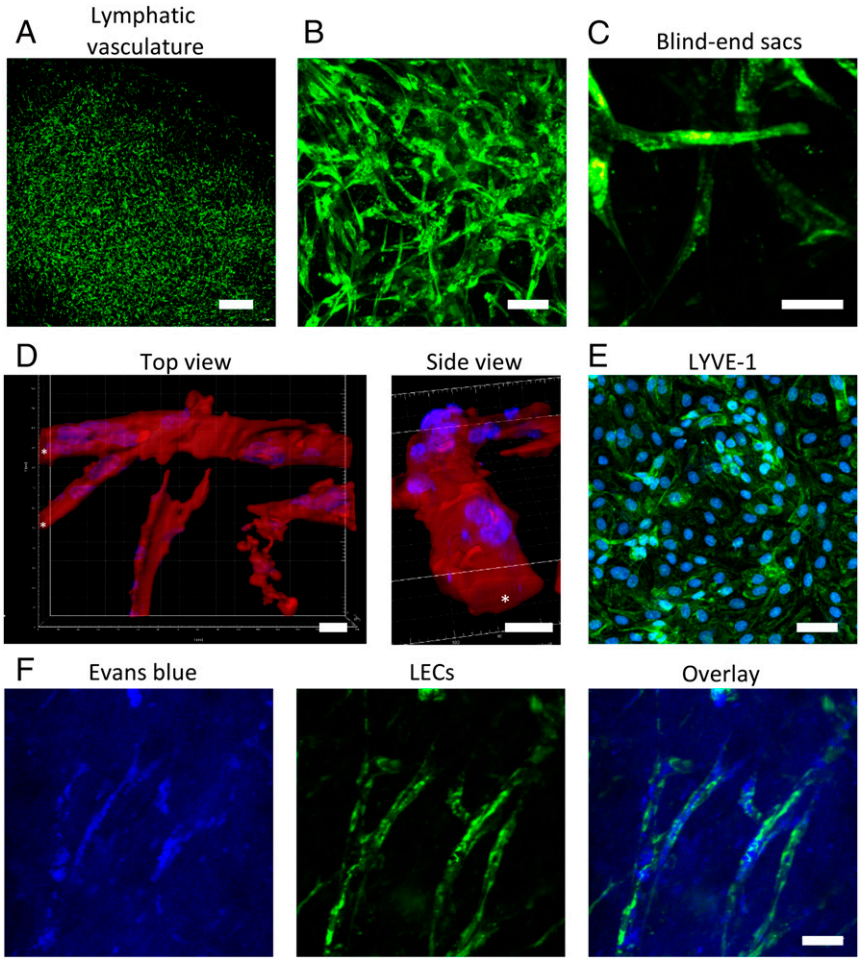

Fig. 4. LEC characterization. (*A*) Coculture of ZsGreen-expressing LECs with DPSCs resulted in lymphatic vessel formation. (Scale bar, 1,000 μm.) (*B*) High-magnification of the lymphatic vasculature. (Scale bar, 100 μm.) (*C*) Vasculature exhibits lymphatic characteristics with the presence of blind-end sacs. (Scale bar, 50 μm.) (*D*) Imaris reconstruction images demonstrate lumen formation within the engineered lymphatic vessels. (Scale bar, 15 μm.) (*E*) LYVE-1 (green) and DAPI (blue) immunofluorescence staining of LECs. (Scale bar, 50 μm.) (*F*) Evans blue (blue) injection into the scaffolds; engineered lymphatic vessels shown in green. (Scale bar, 50 μm.)

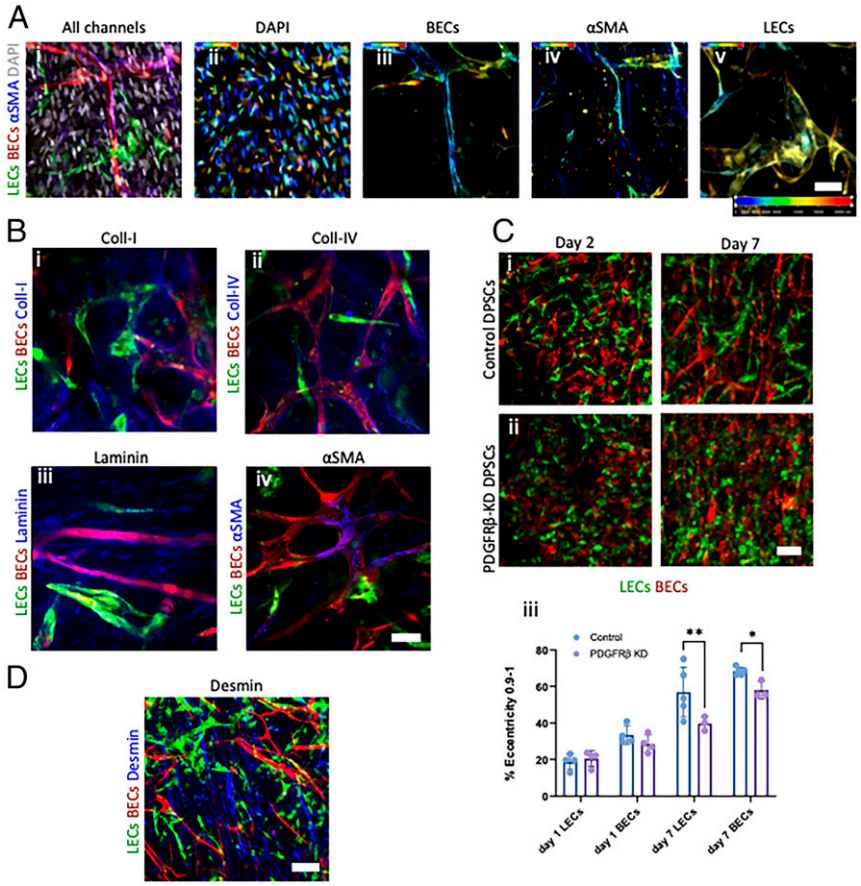

Fig. 5. Multiculture of BECs, LECs, DPSCs, and myoblasts. (*A*, *i*) Maximum-intensity projection of a confocal image of a 7-d construct bearing BECs, LECs, DPSCs, and myoblast and stained for α-SMA. (*ii*–*v*) Color-coded projections of the image presented in *i* split into different channels: (*ii*) DAPI, (*iii*) BECs, (*iv*) α-SMA, and (*v*) LECs. Cool/warm colors indicate near/far from the surface, respectively. (Scale bar, 50 μm.) (*B*) Confocal images of immunofluorescence staining of collagen-I and -IV, laminin, and α-SMA in lymphatic and blood vessel constructs grown for 7 d. (Scale bar, 50 μm.) (*C*) Coculture of LECs and BECs with (*i*) DPSCs and (*ii*) PDGFR-β-KD DPSCs. (*iii*) Eccentricity analysis demonstrating both lymphatic and blood vessel quality. (Scale bar, 100 μm.) (*D*) Whole-mount staining of desmin in constructs composed of LECs, BECs, DPSCs, and myoblasts. (Scale bar, 50 μm.) Error bars show SEM. $*P < 0.05$, $**P < 0.01$.

Fig. S7). Analysis of enriched pathways revealed that significantly up-regulated proteins in the BECs group were associated with response to external stimulus and mechanical stimulus, tissue remodeling, and ECM, whereas in the LECs group, up-regulated proteins were associated with the cytoskeleton, cell motility, membrane organization, and cell polarity (Fig. 6*D*).

Engineered Lymphatic Vessels Integrate In Vivo and Anastomose with Host Lymphatic Vessels. To assess the ability of the engineered lymphatic vessels to anastomose to the host lymphatic vessels and serve as a possible treatment for lymphedema, LEC-DPSC constructs cultured for 7 d with mature and aligned lymphatic vessels were implanted in mice with a defect in the abdominal wall muscle. Mice were euthanized on day 7 after implantation, and whole-mount staining was performed on the grafts. Mouse lymphatic markers (mCD31 and mLYVE1) showed engraft wrapping and end-to-end connections between the host and the implanted lymphatic vessels (Fig. 7 *A* and *B*). Implantation of cyclically stretched constructs resulted in the invasion of the host lymphatic vasculature in the same alignment of the implanted vasculature (Fig. 7*C*).

Discussion

Engineering functional lymphatic vessels holds great promise for treating various conditions involving the lymphatic system, such as to rescue cardiac tissue postmyocardial infarction, improve dermal skin grafts, and relieve lymphedema symptoms. Engineered lymphatic vessels can also serve as in vitro disease models and drug testing systems, enabling the enhanced study of inflammatory responses, cancer, and other processes involving the lymphatic system (18). Despite its great potential in medicine and tissue engineering, research of lymphatic vessel engineering is scarce compared to blood vessel engineering research.

This study investigated the effect of the cellular environment, supporting cells, and mechanical stimulation on lymphatic vessel development and organization. We established a method to create functional engineered lymphatic vessels by coculturing LECs with DPSCs. The resulting vessels were able to uptake fluid and connected to the host lymphatic system upon implantation. Engineered blood vessels were also successfully incorporated into the constructs. The combination of lymphatic and blood vessels in engineered constructs can advance engineered tissue complexity and functionality.

Previous studies have investigated coculture of LECs with fibroblasts. In one method, Gibot et al. seeded LECs on top of collagen-rich fibroblast cell sheets and stacked LEC/fibroblast sheets on top of each other to generate stable lymphatic vessels (10), a procedure that took 42 d. In another method, LECs and adipose-derived stromal cells were cocultured in fibrin scaffolds for 4 wk to create a stable vessel network (12).

In our work, coculturing LECs with DPSCs resulted in the rapid formation of stable lymphatic vessels within a few days. This time frame was similar to that required to form a blood vessel network

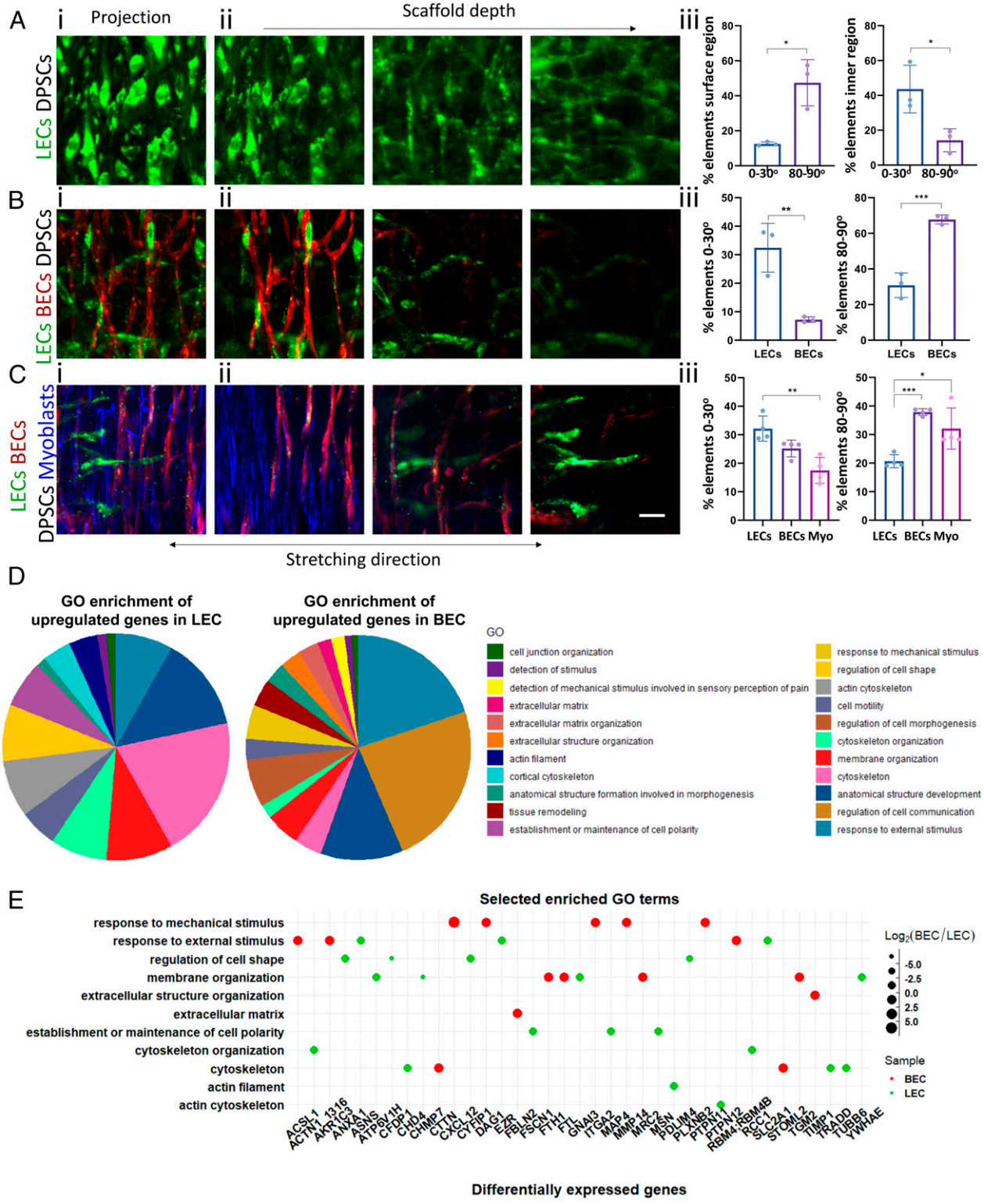

Fig. 6. Cyclic stretch affects lymphatic and blood vessel orientation. (*A*) LEC and DPSC construct under cyclic stretch: (*i*) representative maximum-intensity projection image, (*ii*) representative images of different slices in the *z*-plane (~20-μm intervals), and (*iii*) vessel element orientation with respect to the stretching direction on the construct surface and inner regions. (Scale bar, 200 μm.) (*B*) Constructs of multicultured LECs and BECs with DPSCs. (Scale bar, 200 μm.) (*C*) Constructs of multicultured LECs, BECs, DPSCs, and myoblasts, presented as in *A*. (Scale bar, 50 μm.) (*D*) Pie plots of enriched gene ontology (GO) terms of statistical differentially expressed proteins in LEC-DPSC and BEC-DPSC constructs. (*E*) Select enriched GO terms with their differentially expressed proteins. The size of the point reflects the log2 fold change between BECs and LECs; green (LECs) and red (BECs) colors represent negative and positive values of the fold change in logarithmic scale, respectively. Error bars show SEM. $*P < 0.05$, $**P < 0.01$, $***P < 0.001$.

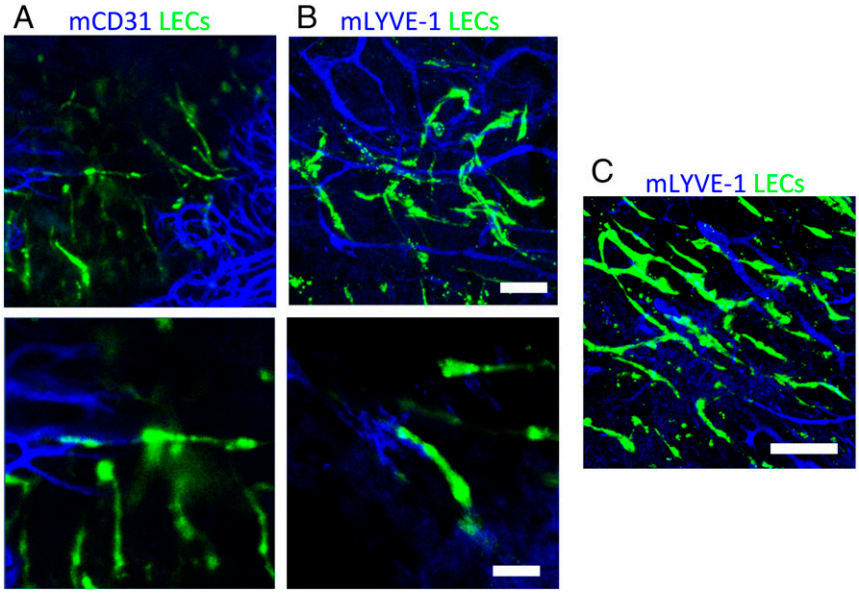

Fig. 7. Implantation of a construct bearing engineered lymphatic vasculature. LEC-DPSC constructs were implanted into a defect in the mouse abdominal wall. After 7 d, mice were euthanized and constructs were stained for mouse lymphatic markers (*A*) anti-mCD31 (blue) and (*B*) anti-mLYVE-1 (blue), which demonstrated anastomosis of engineered lymphatic vessels (green) with host lymphatic vessels. (*Upper* scale bar, 100 μm.) (*Lower* scale bar, 50 μm.) (*C*) Implanted cyclically stretched constructs stained with anti-mLYVE-1 (blue). (Scale bar, 200 μm.)

from BEC and DPSC cocultures (13), while blood vessel networks generated from BEC and fibroblast coculture took longer to form (19). Moreover, the LEC and fibroblast coculture formed poor lymphatic vessels. A possible explanation may be excessive ECM secretion and high tension in the cell environment (indicated by holes in the ECM) in the LEC-fibroblast culture, which may be unconducive to lymphatic vessel formation. Alternatively, the secreted VEGF-A, leptin, and Ang-2 levels may have led to the differences in network stability. VEGF-A secretion was higher in LEC-DPSC as compared to LEC-fibroblast cocultures. Moreover, inhibition of VEGFR-2 in LEC-DPSC constructs by SU5416 hindered lymphatic vessel formation. A previous report showed that VEGF-A inhibition inhibited LYVE-1 outgrowth upon injury and that lymphangiogenesis was reduced in VEGF-A164/164 transgenic mice (20). On day 4, LEC-DPSC coculture also had higher leptin secretion, which was previously shown to increase secretion of VEGF-C, an important mediator in lymphangiogenesis (21). Ang-2 secretion on day 7 was higher in the LEC-fibroblast culture, in accordance with Wu et al. that showed that in the absence of VEGF-A, Ang-2 leads to lymphatic vessel regression (22). Surprisingly, HGF secretion was also higher in the LEC-fibroblast construct. As HGF was previously shown to induce LEC migration, proliferation, and vessel formation (23), the measured increase in its secretion does not correlate with our results that show fewer lymphatic vessels in the LEC-fibroblast coculture, though inhibition of HGF-R in LEC-DPSC constructs resulted in impaired lymphatic vessel formation, indicating its important role in lymphangiogenesis, suggesting a need for further investigation.

Previous studies have shown the importance of PDGFR-β in lymphangiogenesis induction. PDGF-AB and PDGF-BB are ligands that activate PDGFR-β, while PDGF-AA does not activate the receptor. PDGF-AA, -AB, and -BB applied to mouse corneas induced corneal lymphangiogenesis, but PDGF-AA produced inferior lymphatic vasculature compared with PDGF-AB and -BB. This emphasizes the vital role of PDGFR-β in inducing lymphangiogenesis. Moreover, PDGF-BB has been shown to stimulate LEC motility and MAP kinase activity in vitro and to induce lymphangiogenesis in vivo (24).

In our analysis of the role of PDGFR-β in lymphangiogenesis, PDGFR-β KD in LECs-DPSCs coculture resulted in impaired vessel network formation by both LECs and BECs, with fewer interconnected vessels and an increased number of LECs and BECs in single-cell morphology. Cytokine secretion profiling further supported the importance of PDGFR-β, as secretion levels of the prolymphangiogenesis factors VEGF-A, angiogenin, and HGF were lower in PDGFR-β-KD than in wild-type LEC-DPSC cocultures. Furthermore, α-SMA was present in a thin and disorganized form in the KD cultures, consistent with the finding that PDGF-BB promotes α-SMA expression in human retinal pigment epithelial cells (25). PDGF-BB was also shown to stimulate the activation of cofilin, which plays a role in actin cytoskeleton turnover during cell motility (26). Another study supporting our findings showed that PDGFR-β promoted α-SMA expression in vascular smooth muscle cells and in pericytes that were recruited during embryonic blood vessel formation in mice (27). Wild-type LEC-DPSC cocultures also showed collagen-I and -IV expression restricted to the lymphatic vessels, corresponding to the localization of collagen-IV at the lymphatic vessel basement membrane in native lymphatic vessels (28). In contrast, the PDGFR-β-KD constructs showed unbounded collagen-I and -IV fibers, indicating an impaired phenotype of the forming vessels. Moreover, RNA-seq analysis highlighted the importance of PDGFR signaling in lymphangiogenesis as this was found to be one of the most enriched pathways in the up-regulated genes of the LEC-DPSC coculture group. RNA-seq enrichment analysis of up-regulated genes within the coculture group also revealed the involvement of VEGFR3 and beta1 and 3 integrin cell-surface interaction, which corroborated with previous studies that showed that VEGFR3 and beta1 and 3 integrin play a critical role in lymphangiogenesis (29–31). Enriched pathways of down-regulated genes were associated with impaired lymph vessel formation, which correlated with the observed failure of LECs to form vessels in the absence of DPSCs.

Subjecting the engineered lymphatic vessels to cyclic stretching resulted in an interesting phenomenon. On the scaffold surface, lymphatic cells did not form vessels and remained as single cells aligned perpendicularly to the stretching direction, whereas BECs in this area formed vessels aligned in the same direction. Deeper

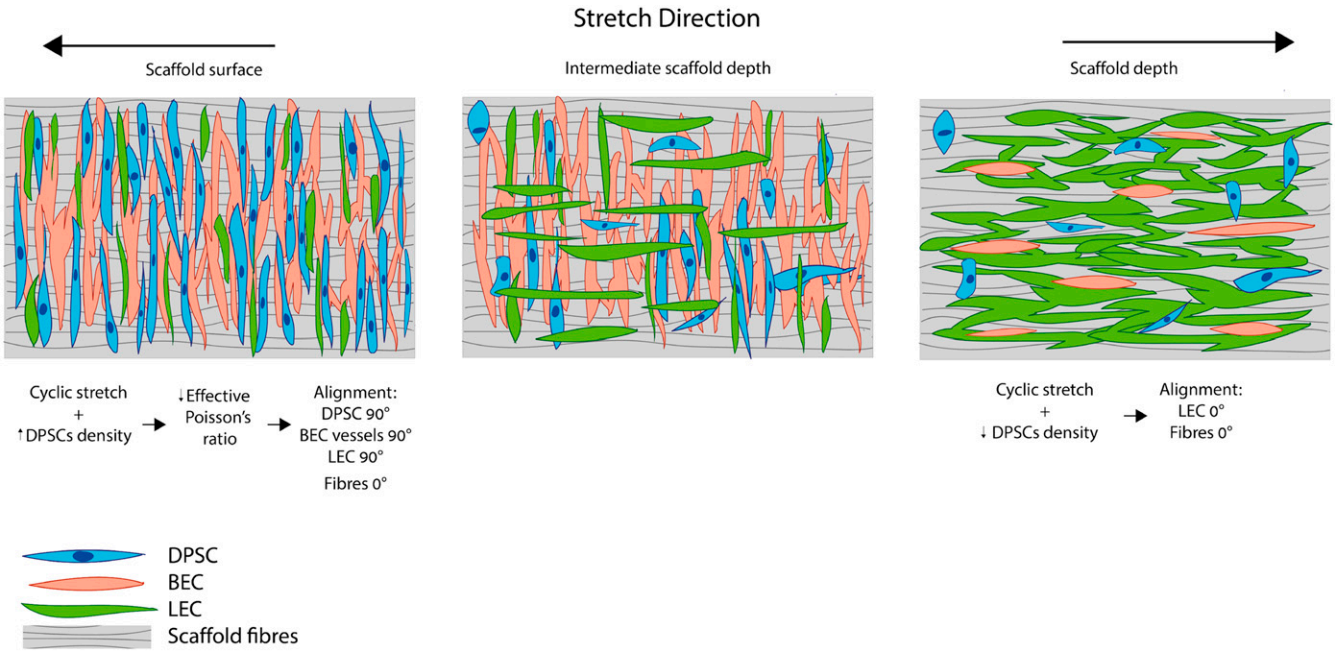

Fig. 8. Cyclic stretch effect on scaffold fiber and lymphatic and blood vessel alignment. The effect of the stretch in the scaffold is divided into three regions. In the surface region, the higher density of supporting cells along with an effective Poisson ratio that approaches zero (14) causes all cells in this region to align perpendicularly to the stretching direction. In the scaffold depth, lymphatics align parallel to the stretching direction as fewer DPSCs are present; thus, cells cannot align in the perpendicular direction. The forming lymphatic vessels sense only the scaffold fibers that align in parallel to the stretching direction (14) and guide their alignment in the same manner.

in the scaffold, LECs formed vessels that primarily aligned parallel to the applied stretch while BEC vessels maintained the same perpendicular orientation. We assume that cells on the surface do not experience the same conditions as the cells deeper within the scaffold. Recently, Huycke et al. published a study characterizing the mechanical regulation of smooth muscle in the intestine during development (32) and separately examined two layers of the gut. The smooth muscle of the inner part of the gut aligns circumferentially; during development, this layer contracts and causes the outer muscle layer to align longitudinally. In our study, the surface and inner regions of the tissue construct also exhibited differential responses, albeit in a different manner. We have previously shown that the surface region of an engineered vascularized tissue consists of a dense layer of supporting cells (33) and that support cell density must be above a certain threshold to cause endothelial cells to align perpendicularly in response to cyclic stretching (15). This correlated with the proteome analysis that showed enriched pathways associated with the detection of external mechanical stimuli. We hypothesize that the LECs on the scaffold surface cannot form vessels due to the extensive density of the supporting cells and resulting ECM on the surface. As a result, only LECs that migrate to the inner part of the scaffold form vessels, which correlates with the proteome analysis that showed enrichment of genes associated with cell motility, membrane organization, and cytoskeleton in the LEC constructs. Moreover, since LECs and supporting cells in the inner region area were highly scattered, they cannot directly sense the cyclic stretching but likely sense and follow the scaffold's aligned fibers, as we have previously shown under static stretch conditions (17) (Fig. 8), and which correlates with the enrichment of genes associated with cell polarity in LEC constructs.

Surgical approaches for treating lymphedema include flap transfer, lymph node transfer, and lymphatic bypass (34, 35). These approaches have varying efficacy, and some have not yet been tested in long-term or well-controlled studies. In addition, some approaches are only suitable for early-stage lymphedema. Our work showed that engineered lymphatic vessels contained lumens and were able to uptake fluid from their surroundings. Moreover, implantation of engineered lymphatic tissue anastomosed to the host lymphatic vasculature. These engineered lymphatic vessels may be applicable for enhancing supermicrosurgical lymphaticovenular anastomosis, a sophisticated surgical technique in which precise anastomoses are performed between lymphatics and venules. The anastomoses create additional outflow conduits to improve lymphatic drainage, and the technique has been used to treat varying stages of lymphedema with good efficacy (36). Implantation of engineered lymphatic vessels around the surgically anastomosed lymphatics and venules may increase the overall number of anastomoses between the lymphatic and venous systems, thus increasing lymphatic drainage.

To summarize, we have developed a fast and simple method for engineering lymphatic vasculature, which can serve as a platform for investigating fundamental questions in lymphangiogenesis both in vitro and in vivo. This work is a promising step toward advancing the treatment of lymphedema and other diseases related to the lymphatic system.

Materials and Methods

Cell Culture. Human LECs (ScienceCell) and human adipose microvascular endothelial cells (HAMECs; ScienceCell) were transduced with ZsGreen and dTomato fluorescent protein using lentivirus (described in *Lentivirus Packaging and LEC and HAMEC Transduction with ZsGreen and dTomato Fluorescent Proteins*). The cells were cultured in endothelial cell medium (ScienceCell) supplemented with 5% fetal bovine serum (FBS; ScienceCell) and endothelial cell growth supplements (ScienceCell). LECs were expanded for up to five to six passages; HAMECs were expanded for up to five to nine passages.

Neonatal normal human dermal fibroblasts (Lonza Walkersville Inc.) were grown in Dulbecco's modified Eagle's medium (DMEM; Gibco), supplemented with 10% FBS (HyClone), 1% nonessential amino acids (NEAA; Gibco), 0.2% β-mercaptoethanol (Sigma-Aldrich), and 1% penicillin-streptomycin solution (PEN STREP) (Biological Industries).

DPSCs (Lonza) were cultured in low-glucose DMEM (Gibco), supplemented with 10% FBS (HyClone), 1% NEAAs (Gibco), 1% GlutaMAX (Gibco), and 1%

PEN STREP-nystatin solution (Biological Industries). Human myoblasts (ScienceCell) were grown in skeletal muscle cell medium (ScienceCell).

Three dimensional vascularized constructs were obtained by coseeding LECs ($2 \cdot 10^5$ cells) with and without HAMECs ($1 \cdot 10^5$ cells) and DPSCs ($6 \cdot 10^5$ cells) or fibroblasts ($6 \cdot 10^5$ cells) in 20 μL medium on CelGro scaffolds (Orthocell) or in 7 μL fibrin on poly(lactide-coglycolide) (PLGA) and poly(L-lactide) (PLLA) scaffolds, followed by a 30-min incubation before the addition of medium. Constructs were supplemented with VEGF-C (R&D, 100 ng/mL).

Inhibitors. To block receptor-ligand interactions, SU5416 (Sigma-Aldrich, 2.1 μM), anti-angiogenin, and anti-hepatocyte growth factor receptor (HGFR) antibodies (R&D, 10 μg/mL) were used. Inhibitors were added to the culture medium of constructs seeded with LECs and DPSCs, which was changed daily. On day 7 of culture, constructs were imaged using a confocal microscope, and images were analyzed using Angiotool software.

Lentivirus Packaging and LEC and HAMEC Transduction with ZsGreen and dTomato Fluorescent Proteins. The Lenti-X HTX Packaging System (fourth generation; Clontech) was used to generate recombinant, replication-incompetent VSV-G pseudotyped lentiviruses, according to the manufacturer's instructions. Transfection of the expression vector into the Lenti-X 293T packaging cells (Clontech) was performed in a Lenti-X HTX packaging mix. The supernatants of transfected packaging cells were collected 72 h later and filtered through a 45-μm filter before being added to the cells, with 6 mg/mL polybrene (Sigma-Aldrich). The transduction medium was replaced by a culture medium 24 h thereafter, and cells were then cultured for 72 h to allow gene product accumulation in the cells. Cells were then selected using 1 mg/mL puromycin (Takara Bio Company).

Electroporation-Mediated CRISPR Editing of DPSCs. Specific guide RNAs (gRNAs) were generated using the CHOPCHOP web tool and the Guide-It Complete In Vitro single guide RNA (sgRNA) Screening System (Clontech, 632636). Several gRNAs were tested to find the most efficient one, followed by Sanger sequencing (3500xL Genetic Analyzer, Life Technologies).

The sgRNA Sequence Cloned Was: GTAAGGGGCCATGTAGTTGG. DPSCs were seeded in 12-well plates at a density of 2×10^6 cells per well. After 24 h, the cells were transiently transfected with 1 μg Cas9 (Clontech) and 0.5 μg gRNA using lipofectamine 2000 (Invitrogen) as per the manufacturer's protocols. Electroporation was performed using the Neon electroporator, according to the Clontech user manual for Cas9 (1,400 V, 20 ms, 2 pulses). Genomic DNA was extracted 48 h after transfection, using the Mutation Detection Kit (Clontech) after electroporation. A resolvase reaction was performed on the samples to verify the editing; samples showing unsuccessful editing were discarded (*SI Appendix*, Fig. S1).

Protein Extraction and Immunoblotting. Both wild type and PDGFR-β-KD DPSCs were washed with phosphate buffered saline (PBS) and placed in a single tube containing radioimmunoprecipitation assay solution (Sigma-Aldrich) and protease inhibitors mixture (Sigma-Aldrich). Constructs were homogenized, and the total protein content was determined using the Bradford method (Bio-Rad). Proteins were separated on a 4 to 12% SDS-PAGE (sodium dodecyl sulphate–polyacrylamide gel electrophoresis) gel (NuPage, Life Technologies) and transferred to a nitrocellulose membrane (Bio-Rad). After blocking with 5% nonfat milk (Bio-Rad), the membranes were immunoblotted (overnight, at 4 °C) with primary antibodies: 1:2,000 goat anti–PDGFR-β (R&D) and 1:1,000 mouse anti-GAPDH (Santa Cruz) diluted in blocking buffer. The bound antibodies were detected following incubation with horseradish peroxidas–conjugated anti-mouse/goat IgG (GE Healthcare Life Sciences), followed by exposure to the enhanced chemiluminescence Western blotting system (ECL; Amersham Biosciences). Images were acquired with the LAS-3000 imaging system (FujiFilm). Dense cytometry analysis was performed using multigauge software (Bioz). Data are presented relative to GAPDH.

Scaffolds and Mechanical Stimulation. CelGro scaffolds (Orthocell) were cut to 1 × 0.5 cm. Mechanical stimulation was applied to the constructs 1 d post-seeding using an EBERS TC-3 bioreactor, with uniaxial oscillatory (sinusoidal) stretching at 20% strain and 1 Hz frequency, for 21 d.

PLLA/PLGA scaffolds were prepared as follows: 0.4 g NaCl particles were covered with 0.24 mL PLLA/PLGA solution, which was dissolved in chloroform and evaporated overnight. Salt was then leached out by four washes, leaving pores within the scaffold. Scaffolds were then cut into 6-mm diameter circles of 0.8-mm thickness.

Fibrin gel was obtained by mixing thrombin (20 U/mL, Sigma-Aldrich) with fibrinogen (15 mg/mL, Sigma-Aldrich).

Whole-Mount Staining, Evans Blue Assay, and Imaging. Constructs were fixed with paraformaldehyde (4%), for 20 min, and then permeabilized with 0.3% Triton X-100 (Bio-Lab Ltd.), for 10 min. Constructs were then washed with PBS and immersed overnight in Bovine serum albumin solution (5%; Millipore). Samples were then incubated with the following primary antibodies overnight at 4 °C: mouse anti–human-LYVE (1:200; R&D Systems), rat anti–mouse-LYVE (1:100; Santa Cruz), and anti-human desmin (1:50; Dako). Constructs were then treated with Alexa 647-donkey anti-rat (1:400) or Cy3-donkey anti-mouse (1:100; Jackson Immunoresearch Laboratory) secondary antibodies and DAPI (Sigma-Aldrich) for 3 h, at room temperature. Evans blue was injected into the vascularized construct using an insulin needle, followed by 10 min incubation, after which constructs were imaged.

Whole vascularized constructs were imaged with a confocal microscope (LSM700, Zeiss), using 2.5×, 5×, 20×, and 63× oil immersion lenses. All image analyses were quantified using self-written algorithms in MATLAB that transformed captured images into binary images prior to analysis.

Proteomics. For the proteomics experiments, cocultures of DPSCs with LECs and of DPSCs with BECs were seeded into Gelfoam scaffolds (Pfizer) and subjected to cyclic stretch. After 14 d of culture, constructs were digested by trypsin, analyzed by liquid chromatography–mass spectrometry on a Q-Exactive plus (Thermo), and identified by Maxquant (Mathias Mann's laboratory, Max Planck Institute) software against the human proteome—part of the Uniprot database and a decoy database (in order to determine the false discovery rate [FDR]). Quality control was performed on the proteomics data, and only proteins with 2 Razor + unique peptide and above were further analyzed, to increase the certainty of protein identification. *t* test was performed on the normalized intensities between the two coculture groups (DPSCs with BECs versus DPSCs with LECs). Significant differentially expressed protein levels between the two groups were defined as proteins with at least 3 ms/ms count and FDR adjusted *P* value below 0.05. In total, 147 proteins with statistical expression differences were detected between BECs and LECs (reference Dataset S1). A heatmap of these proteins was generated based on the *Z*-score of their normalized intensities (*SI Appendix*, Fig. S7), using ComplexHeatmap R package version 2.6.2 (37). All analyses were conducted using R version 4.0.5.

RNA-Seq. Coculture of DPSCs and LECs and monoculture of LECs were seeded onto CelGro scaffolds. After 7 d of culture, constructs were digested with collagenase (5 mg/mL, Sigma-Aldrich) and then subjected to flow cytometry ARIA–IIIU sorting to enrich the endothelial cells in the coculture group. RNA was then extracted using the Qiagen RNA extraction kit.

RNA libraries were generated using SMARTer Stranded Total RNA-Seq Kit v2 - Pico Input Mammalian Prep Kit (Takara), according to manufacturer's protocol, and sequenced with Illumina NextSeq550, 75 single-end run. The number of reads ranged from 48,359,119 to 76,784,334 per sample. The reads were mapped to the human genome (*GRCm38*) using Tophat2 version 2.1.0 (38), with up to three mismatches allowed per read. The minimum and maximum intron sizes were set to 50 and 100,000, respectively, and an annotation file was provided to the mapper. The percentage of uniquely mapped reads ranged from 48 to 62.3% per sample. Only uniquely mapped reads were counted to genes, using "HTSeq-count" package version 0.11.2 with "union" mode (39). Normalization and differential expression analyses were conducted using DESeq2 R package version 1.28.1 (40). Sample preparation, sequencing, quality control, and initial bioinformatic analyses were conducted by the "Technion Genome Center," Life Science and Engineering Interdisciplinary Research Center, Technion, Haifa, Israel. A heatmap was generated with the Heatmapper tool, and enriched pathways were found with the enrichr tool (41).

In Vivo Implantation. The animal study was approved by the animal experiments ethics committee of the Technion. Female athymic nude mice (7 to 9 wk old; Harlan Laboratories) were anesthetized using a ketamine:xylazine mixture at a dose of 35 μL/20 g. To access the linea alba, a small incision was made, followed by creation of a circular wound by cutting a full-thickness tissue section from the linea alba. Next, lymphatic grafts were sutured in place using four 8-0 silk sutures; skin was sutured with 4-0 silk sutures. After 7 d, anti-mouse CD31 (BioLegend) was injected into the tail vein. Mice were then euthanized, after which the graft area was excised and fixed in 10% formalin (Sigma-Aldrich). The graft area was imaged immediately after the

excision using a confocal microscope, followed by whole-mount staining of the graft with anti-mouse LYVE antibody.

Statistical Analysis. Presented data include the mean ± SEM (SEM). A two-way ANOVA was performed to examine the influence of two independent categorical variables, followed by Bonferroni's multiple comparison tests. Results were considered significant for $P < 0.05$. Statistical analyses were performed using GraphPad Software.

Data Availability. All study data are included in the article and/or supporting information.

ACKNOWLEDGMENTS. This project has received funding from the European Research Council under the European Union's Horizon 2020 research and innovation program (Grant Agreement No. 818808). We thank Dina Safina for proofreading the manuscript.

1. M. A. Swartz, The physiology of the lymphatic system. *Adv. Drug Deliv. Rev.* **50**, 3–20 (2001).
2. M. S. Pepper, M. Skobe, Lymphatic endothelium: Morphological, molecular and functional properties. *J. Cell Biol.* **163**, 209–213 (2003).
3. A. A. Grada, T. J. Phillips, Lymphedema: Pathophysiology and clinical manifestations. *J. Am. Acad. Dermatol.* **77**, 1009–1020 (2017).
4. M. E. Nipper, J. B. Dixon, Engineering the lymphatic system. *Cardiovasc. Eng. Technol.* **2**, 296–308 (2011).
5. W. L. Olszewski, Contractility patterns of human leg lymphatics in various stages of obstructive lymphedema. *Ann. N. Y. Acad. Sci.* **1131**, 110–118 (2008).
6. J. W. Baish, C. Kunert, T. P. Padera, L. L. Munn, Synchronization and random triggering of lymphatic vessel contractions. *PLoS Comput. Biol.* **12**, e1005231 (2016).
7. A. W. Caulk, Z. V. Nepiyushchikh, R. Shaw, J. B. Dixon, R. L. Gleason Jr, Quantification of the passive and active biaxial mechanical behaviour and microstructural organization of rat thoracic ducts. *J. R. Soc. Interface* **12**, 20150280 (2015).
8. D. Marino, J. Luginbühl, S. Scola, M. Meuli, E. Reichmann, Bioengineering dermoepidermal skin grafts with blood and lymphatic capillaries. *Sci. Transl. Med.* **6**, 221ra14 (2014).
9. L. Gibot *et al*., Cell-based approach for 3D reconstruction of lymphatic capillaries in vitro reveals distinct functions of HGF and VEGF-C in lymphangiogenesis. *Biomaterials* **78**, 129–139 (2016).
10. L. Gibot *et al*., Tissue-engineered 3D human lymphatic microvascular network for in vitro studies of lymphangiogenesis. *Nat. Protoc.* **12**, 1077–1088 (2017).
11. C. L. Helm, A. Zisch, M. A. Swartz, Engineered blood and lymphatic capillaries in 3-D VEGF-fibrin-collagen matrices with interstitial flow. *Biotechnol. Bioeng.* **96**, 167–176 (2007).
12. L. Knezevic *et al*., Engineering blood and lymphatic microvascular networks in fibrin matrices. *Front. Bioeng. Biotechnol.* **5**, 25 (2017).
13. S. Guo *et al*., Prevascularized scaffolds bearing human dental pulp stem cells for treating complete spinal cord injury. *Adv. Healthc. Mater.* **9**, e2000974 (2020).
14. Y. Cao, Direct role of PDGF-BB in lymphangiogenesis and lymphatic metastasis. *Cell Cycle* **4**, 228–230 (2005).
15. S. Landau, S. Ben-Shaul, S. Levenberg, Oscillatory strain promotes vessel stabilization and alignment through fibroblast YAP-mediated mechanosensitivity. *Adv. Sci. (Weinh.)* **5**, 1800506 (2018).
16. D. Rosenfeld *et al*., Morphogenesis of 3D vascular networks is regulated by tensile forces. *Proc. Natl. Acad. Sci. U.S.A.* **113**, 3215–3220 (2016).
17. S. Landau *et al*., Tissue-level mechanosensitivity: Predicting and controlling the orientation of 3D vascular networks. *Nano Lett.* **18**, 7698–7708 (2018).
18. L. Alderfer, A. Wei, D. Hanjaya-Putra, Lymphatic tissue engineering and regeneration. *J. Biol. Eng.* **12**, 32 (2018).
19. S. Ben-Shaul, S. Landau, U. Merdler, S. Levenberg, Mature vessel networks in engineered tissue promote graft-host anastomosis and prevent graft thrombosis. *Proc. Natl. Acad. Sci. U.S.A.* **116**, 2955–2960 (2019).
20. C. Cursiefen *et al*., VEGF-A stimulates lymphangiogenesis and hemangiogenesis in inflammatory neovascularization via macrophage recruitment. *J. Clin. Invest.* **113**, 1040–1050 (2004).
21. W. H. Yang *et al*., Leptin promotes VEGF-C production and induces lymphangiogenesis by suppressing miR-27b in human chondrosarcoma cells. *Sci. Rep.* **6**, 28647 (2016).
22. X. Wu, N. Liu, The role of Ang/Tie signaling in lymphangiogenesis. *Lymphology* **43**, 59–72 (2010).
23. K. Kajiya, S. Hirakawa, B. Ma, I. Drinnenberg, M. Detmar, Hepatocyte growth factor promotes lymphatic vessel formation and function. *EMBO J.* **24**, 2885–2895 (2005).
24. R. Cao *et al*., PDGF-BB induces intratumoral lymphangiogenesis and promotes lymphatic metastasis. *Cancer Cell* **6**, 333–345 (2004).
25. Y. Si, J. Wang, J. Guan, Q. Han, Y. Hui, Platelet-derived growth factor induced alpha-smooth muscle actin expression by human retinal pigment epithelium cell. *J. Ocul. Pharmacol. Ther.* **29**, 310–318 (2013).
26. V. Reyhani *et al*., PDGF-BB enhances collagen gel contraction through a PI3K-PLCγ-PKC-cofilin pathway. *Sci. Rep.* **7**, 8924 (2017).
27. M. Hellström, M. Kalén, P. Lindahl, A. Abramsson, C. Betsholtz, Role of PDGF-B and PDGFR-beta in recruitment of vascular smooth muscle cells and pericytes during embryonic blood vessel formation in the mouse. *Development* **126**, 3047–3055 (1999).
28. N. Vainionpää *et al*., Basement membrane protein distribution in LYVE-1-immunoreactive lymphatic vessels of normal tissues and ovarian carcinomas. *Cell Tissue Res.* **328**, 317–328 (2007).
29. L. Zhang *et al*., VEGFR-3 ligand-binding and kinase activity are required for lymphangiogenesis but not for angiogenesis. *Cell Res.* **20**, 1319–1331 (2010).
30. C. J. Avraamides, B. Garmy-Susini, J. A. Varner, Integrins in angiogenesis and lymphangiogenesis. *Nat. Rev. Cancer* **8**, 604–617 (2008).
31. S. H. Wang *et al*., Laminin γ2-enriched extracellular vesicles of oral squamous cell carcinoma cells enhance in vitro lymphangiogenesis via integrin α3-dependent uptake by lymphatic endothelial cells. *Int. J. Cancer* **144**, 2795–2810 (2019).
32. T. R. Huycke *et al*., Genetic and mechanical regulation of intestinal smooth muscle development. *Cell* **179**, 90–105.e21 (2019).
33. S. Landau, S. Guo, S. Levenberg, Localization of engineered vasculature within 3D tissue constructs. *Front. Bioeng. Biotechnol.* **6**, 2 (2018).
34. B. J. Mehrara, J. C. Zampell, H. Suami, D. W. Chang, Surgical management of lymphedema: Past, present, and future. *Lymphat. Res. Biol.* **9**, 159–167 (2011).
35. R. Deldar *et al*., An alternative approach to combined autologous breast reconstruction with vascularized lymph node transfer. *Microsurgery* **37**, 463–464 (2017).
36. P. J. Hawkes, M. McNurlen, M. Bowen, W. F. Chen, Strategic incision placement to facilitate successful supermicrosurgical lymphaticovenular anastomoses. *Int. Microsurg. J.*, 10.24983/scitemed.imj.2018.00049 (2018).
37. Z. Gu, R. Eils, M. Schlesner, Complex heatmaps reveal patterns and correlations in multidimensional genomic data. *Bioinformatics* **32**, 2847–2849 (2016).
38. C. Trapnell, L. Pachter, S. L. Salzberg, TopHat: Discovering splice junctions with RNA-Seq. *Bioinformatics* **25**, 1105–1111 (2009).
39. S. Anders, P. T. Pyl, W. Huber, HTSeq–A Python framework to work with high-throughput sequencing data. *Bioinformatics* **31**, 166–169 (2015).
40. M. I. Love, W. Huber, S. Anders, Moderated estimation of fold change and dispersion for RNA-seq data with DESeq2. *Genome Biol.* **15**, 550 (2014).
41. E. Y. Chen *et al*., Enrichr: Interactive and collaborative HTML5 gene list enrichment analysis tool. *BMC Bioinformatics* **14**, 128 (2013).